Ultramicroscopy 111 (2011) 518–523

Contents lists available at ScienceDirect

Ultramicroscopy

journal homepage: www.elsevier.com/locate/ultramic

Thermal stability of TiAlN/CrN multilayer coatings studied by atom probe tomography

Pyuck-Pa Choi [a], Ivan Povstugar [a,*], Jae-Pyeong Ahn [b], Aleksander Kostka [a], Dierk Raabe [a]

[a] Max-Planck-Institut für Eisenforschung, Department for Microstructure Physics and Metal Forming, Max-Planck-Strasse 1, 40237 Düsseldorf, Germany
[b] Korea Institute of Science and Technology, Advanced Analysis Center, P.O. Box 131, Cheongryang, 130-650 Seoul, Republic of Korea

ARTICLE INFO

Available online 19 November 2010

Keywords:
Hardcoatings
Multilayers
Thermal stability
Atom probe tomography

ABSTRACT

This study is about the microstructural evolution of TiAlN/CrN multilayers (with a Ti:Al ratio of 0.75:0.25 and average bilayer period of 9 nm) upon thermal treatment. Pulsed laser atom probe analyses were performed in conjunction with transmission electron microscopy and X-ray diffraction. The layers are found to be thermally stable up to 600 °C. At 700 °C TiAlN layers begin to decompose into Ti- and Al-rich nitride layers in the out-of-plane direction. Further increase in temperature to 1000 °C leads to a strong decomposition of the multilayer structure as well as grain coarsening. Layer dissolution and grain coarsening appear to begin at the surface. Domains of AlN and TiCrN larger than 100 nm are found, together with smaller nano-sized AlN precipitates within the TiCrN matrix. Fe and V impurities are detected in the multilayers as well, which diffuse from the steel substrate into the coating along columnar grain boundaries.

1. Introduction

Over the past decades, transition metal nitrides have found a wide-spread application as hardcoating materials for improving wear, oxidation, and corrosion resistance of cutting tools and machine parts [1–16]. Initial research on such nitrides focused on single and multilayers of several micrometers in thickness (TiN, CrN, NbN, VN, etc.) [1–3]. As the properties required for hard-coatings are nowadays far more demanding than those achieved by such thick layers, there is a need for the development of more advanced coating systems. An efficient way of improving the mechanical properties of hardcoatings lies in the preparation of compositionally modulated nanoscale multilayers using physical vapor deposition techniques [4–14]. Maximum hardness values ranging from 3500 to 5000 kg/mm^2 could be achieved in several nitride multilayer systems (e.g. TiN/AlN [5], TiN/NbN [6], TiN/VN [7], TiN/CrN [8,9], AlN/CrN [10–12]). Such a high hardness is comparable to cubic-BN and is only exceeded by diamond. However, nitride multilayer coatings have the advantage that often they not only provide excellent mechanical properties but also high corrosion and oxidation resistance [4,13–16]. On the other hand, one of the main drawbacks of multilayers is their limited thermal stability. Due to the large amount of internal interfaces, multilayers are in a metastable state. In dry-cutting applications, the operation temperatures can exceed 1000 °C resulting in the dissolution of the layered structure, e.g., due to interdiffusion. Such a change in microstructure usually leads to a substantial deterioration of the mechanical properties.

The present study is dedicated to the thermal stability of multi-layered TiAlN/CrN, a high-performance coating system that shows an outstanding combination of wear and oxidation resistance [17]. Several reports exist on the microstructure and mechanical properties of TiAlN/CrN multilayers as well as on their thermal evolution [17–22]. The onset of interdiffusion in TiAlN/CrN is observed at 500 °C while microhardness starts to decrease at 600 °C. When heated up to 900 °C, the coatings undergo oxidation [19]. However, the above-cited reports only present the results of air-annealing experiments, which make it difficult to distinguish between the effects of heating and oxidation on the dissolution of the nanolayers. Furthermore, there is a general lack of information about thermally induced atomic-scale chemical changes occurring in nitride multi-layer coatings. This paper is aimed at elucidating the microstructural evolution of multilayered TiAlN/CrN upon annealing in protective Ar atmosphere so that oxidation can be neglected. Atom probe tomography (APT) was performed in conjunction with transmission electron microscopy (TEM) and X-ray diffraction (XRD).

2. Methods

TiAlN/CrN multilayer samples were prepared by means of reactive sputter-deposition on an M2 high speed steel substrate using high-purity $Ti_{0.75}Al_{0.25}$ and Cr targets and a rotating substrate holder. In order to improve the adherence, CrN and TiAlN buffer

* Corresponding author. Tel.: +49 211 6792 172; fax: +49 211 6792 333.
E-mail address: i.povstugar@mpie.de (I. Povstugar).

0304-3991/$ - see front matter © 2010 Elsevier B.V. All rights reserved.
doi:10.1016/j.ultramic.2010.11.012

layers of about 100 nm thickness were deposited onto the substrate prior to the deposition of multilayer coating. Further details about the sputter-deposition process are described elsewhere [22]. The total thickness of the deposited coating was approximately 2 μm. The Ti to Al ratio of the as-sputtered TiAlN layers determined by wavelength-dispersive electron probe microanalysis (JEOL, JXA-8500F) was 2.8 to 1. According to [22,23], this ratio yields single-phase fcc hardcoatings with superior mechanical properties. To study the thermal stability of multilayer structures, the samples were sealed into quartz tubes under Ar gas atmosphere and annealed at 600, 700, and 1000 °C for 1 h. Structural characterization of initial and annealed samples as well as the determination of the bilayer thickness was done using TEM (JEOL JEM-2200FS, 200 kV, in scanning TEM mode) and XRD (CoK_α radiation, wavelength 0.1788 nm). APT analyses were carried out with an Imago LEAP^{TM} 3000X HR system, applying laser pulses of ~10 ps pulse length, 532 nm wavelength, 0.4 nJ pulse energy, 250 kHz pulse frequency, and 0.5% detection rate. The specimen base temperature was set to 60 K. TEM and APT specimens were prepared using a dual-beam focused ion beam (FEI Helios Nanolab 600), as described in [24,25]. APT samples were prepared from regions about 300 nm below the surface of the coating unless otherwise stated. To reduce the amount of implanted Ga ions, TEM and APT samples were ion-milled at low ion energies (2 and 5 kV, respectively) during the final steps of the preparation. According to the APT mass spectra, the Ga content in the analyzed volume was below 0.01 at% for all specimens.

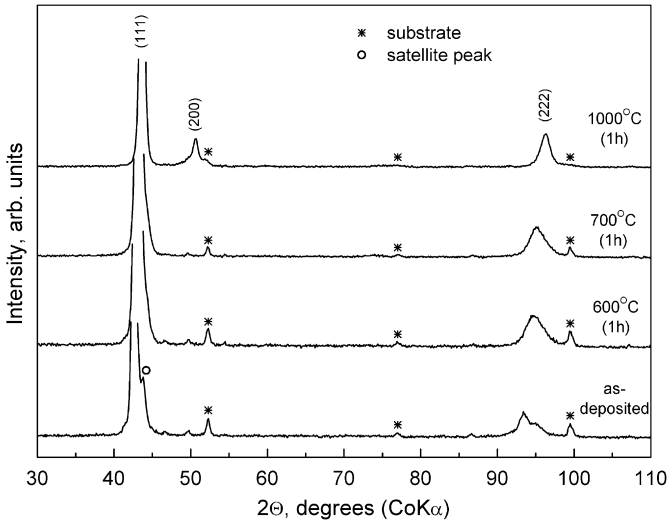

Fig. 1. X-ray diffraction patterns of an as-sputtered sample and samples annealed at 600, 700, and 1000 °C for 1 h.

3. Results and discussion

Fig. 1 shows XRD patterns of an as-sputtered sample as well as of samples annealed at 600, 700, and 1000 °C for 1 h. The most intensive peaks are (1 1 1) and (2 2 2) reflexes of a B1-type fcc structure typical of equilibrium CrN and TiN phases. No other peaks can be detected, suggesting a strong fiber texture. The lattice parameter calculated from the positions of major peaks is 0.427 nm, which is slightly larger than those of fcc CrN (0.414 nm) and TiN (0.424 nm). The difference is attributed to residual compressive stresses [18,19], which are a common feature in sputter-deposited coatings. A satellite peak is observed on the right-hand side of the (1 1 1) peak indicating the presence of a superlattice structure. The estimation of the superlattice period from the position of the satellite peak gives a value of 9.2 ± 0.5 nm. Annealing at 600 °C for 1 h leads to a peak shift towards larger 2Θ angles due to gradual stress relaxation in the multilayer structure. The satellite peak disappears at this temperature indicating that the interfaces between individual layers are not as sharp as those

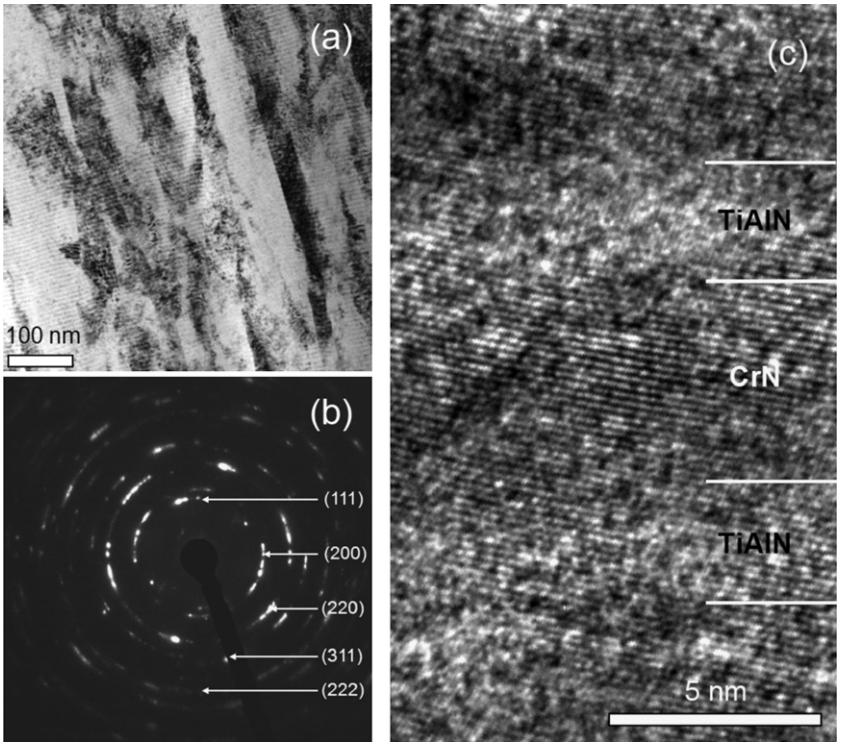

Fig. 2. (a) TEM bright-field image, (b) corresponding selected area diffraction pattern, and (c) high-resolution TEM image of an as-sputtered sample.

in the initial state. An increase in annealing temperature up to 700 °C results in a further gradual shift of the Bragg peaks towards larger angles. After annealing at 1000 °C for 1 h the lattice parameter decreases to a value of 0.417 nm that is between the lattice parameter values of pure CrN and TiN, and (2 0 0) peak emerges. However, no other peaks of B1 structure are distinguishable in the XRD pattern suggesting that the coating remains textured.

Fig. 2(a) and (b) shows a TEM bright-field image of the as-sputtered sample and a selected area diffraction pattern, respectively. The multilayer structure is uniform over the whole thickness of the coating. Columnar grains across several tens of layers can be observed, which is typical of coatings sputter-deposited at temperatures significantly below the melting point. Columnar grain growth is reported to be controlled by the competition between discrete atomic deposition and surface diffusion [26]. Neighboring grains in Fig. 2(a) exhibit diffraction contrast indicating orientation differences. Taking into account the fiber texture observed in the XRD measurements, it can be concluded that the grains are rotated with respect to each other around an axis perpendicular to the surface. In addition, some grains exhibit strong strain contrast, which can be assigned to residual stresses. The diffraction rings in Fig. 2(b) can be identified as B1 fcc reflexes of both TiAlN and CrN. These observations are in good agreement with the XRD results discussed above. Fig. 2(c) shows a high-resolution TEM image of the multilayers. Lattice fringes are continued across layer interfaces, clearly revealing that the neighboring layers are coherent. The average bilayer thickness determined from TEM images gradually increases from 8.3 to 9.5 $\pm$ 0.2 nm, moving from the surface of the coating towards the substrate. These values were used as a reference for the depth calibration of the APT data.

In the APT measurements, Al was detected as Al^+, Al^{2+}, and Al^{3+} ions while Ti was detected as Ti^{2+} and Ti^{3+} ions as well as TiN^{2+} molecules. Cr was detected as Cr^{2+} along with CrN^+ and CrN^{2+}. The fact that Cr and Ti were also detected as nitride complexes, whereas Al was detected only as single ions, which can be explained by the binding energies of the respective metal nitrides. These are 73.8 eV for AlN [27], 396.8 eV for CrN [28], and 454.4 eV for TiN [29]. Fig. 3 shows a concentration depth profile across several layers. Alternating Cr- and TiAl-rich nitride layers can be clearly resolved. Cr and Ti peaks seen in the concentration profiles are slightly asymmetrical, and the orientation of asymmetry does not reverse when the multilayers are analyzed "upside-down". Therefore, this asymmetry is not due to real compositional variations in the sputter-deposited sample but may be ascribed to a difference in evaporation fields of CrN and TiAlN layers. In contrast, the small "shoulders" of the Al peaks and their shift with respect to the Ti peaks reverse when reversing the analysis direction. Therefore, they are not considered as artifacts of APT analyses and may

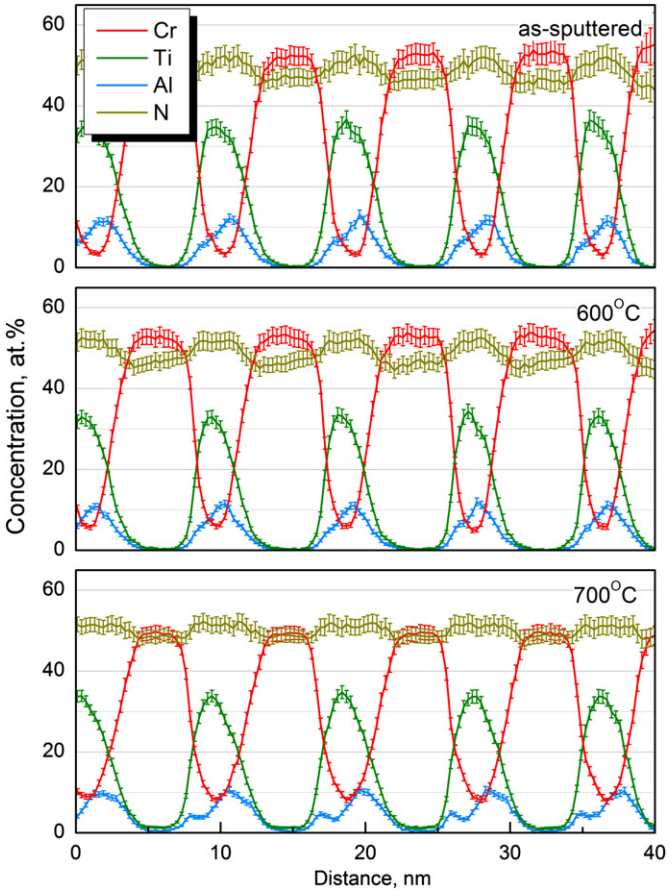

Fig. 3. Concentration depth profiles of elements across multilayers for an as-sputtered sample and samples annealed at 600 and 700 °C for 1 h.

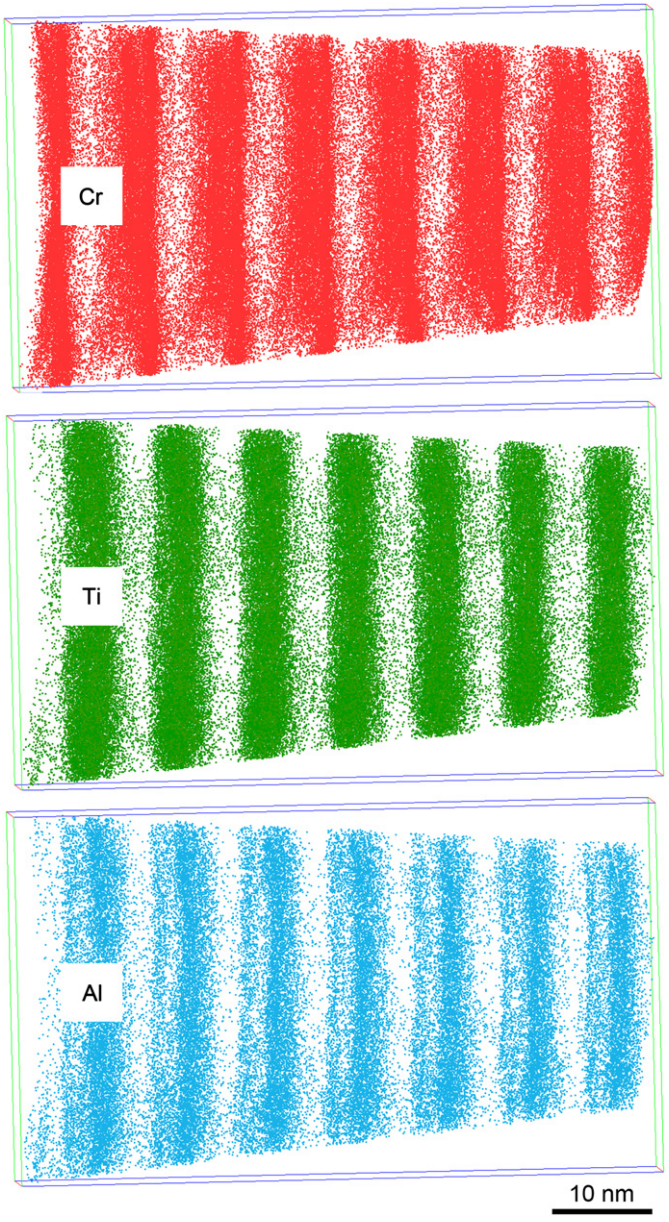

Fig. 4. APT elemental map of Cr, Ti, and Al for a sample annealed at 700 °C for 1 h. Nitrogen atoms are not shown for clarity.

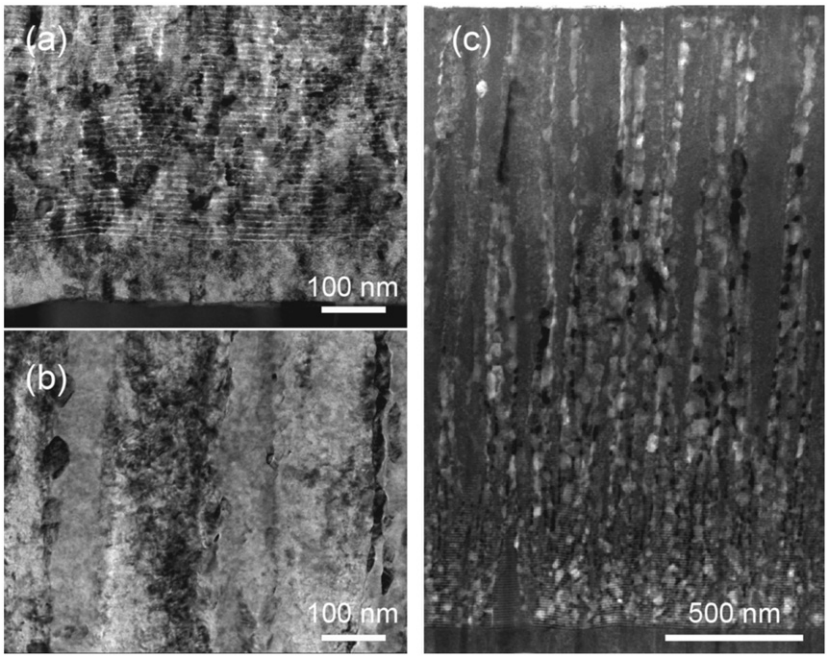

Fig. 5. TEM images of a sample annealed at 1000 °C for 1 h: bright-field images of (a) deep region and (b) near-surface region, and (c) dark-field image of the coating cross-section.

originate from a slight decomposition of the TiAlN layers occurring in the course of the sputter-deposition process itself, as the substrate temperature is kept at 300 °C. The measured compositions of both TiAlN and CrN slightly deviate from 50:50 ratio where the average composition of the CrN layers amounts to 53 at% Cr and 47 at% N (no traces of Ti and Al) and the TiAlN layers to 35 at% Ti, 11.5 at% Al, 3.5 at% Cr, and 49 at% N. This discrepancy in the nitrogen content is not surprising as the composition of the nitride layers prepared by reactive ion sputtering is expected to depend on the Ar and N_2 gas pressure as well as on the target material. The average Ti to Al ratio of the TiAlN layers, as measured by APT, is 3.0 to 1, which is in good agreement with electron probe microanalysis results. A small amount of Cr found within the TiAl-rich nitride layers can be attributed to the diffusion of Cr into underlying TiAlN layers during the deposition process.

Although XRD results indicate that layer interfaces become more diffuse on annealing at 600 °C, no significant compositional changes are observed at this temperature by means of APT (see Fig. 3). Therefore, we conclude that the studied hardcoatings have relatively high stability in this temperature range with short-range diffusion occurring only at the interfaces. Due to the inaccuracy in reconstructing layers with different evaporation fields and detection of complex ions, such short-range diffusion may not be resolved by APT. As shown in Fig. 2(c), the TiAlN/CrN multilayers form coherent interfaces. Due to this coherency, the interfacial energy and the driving force for layer dissolution may be low. Kinetic reasons for thermal stability of the layered structure should be considered as well. Transition metals are known to have a high melting point and usually low diffusion coefficients for metal diffusion [30]. Therefore, diffusion-controlled processes such as decomposition can be suppressed in nitride hardcoatings especially at lower temperatures. To our knowledge however, there is no published diffusion data for the TiAlN/CrN system to verify our results.

Decomposition of the multilayered structure starts at 700 °C as observed from the concentration depth profiles and APT elemental maps presented in Figs. 3 and 4, respectively. CrN layers remain intact while TiAlN layers decompose into a Ti-rich and two Al-rich layers (see Figs. 3 and 4) in the direction perpendicular to the layers. The type of decomposition for a single-layered $Ti_{100-x}Al_xN$ compound (with $x=0.5$ and 0.66) was shown to be a spinodal decomposition process, using XRD, TEM, and APT [31,32]. From first-principles calculations of the mixing enthalpy for the pseudo-binary TiN–AlN system [33,34], it could be concluded that $Ti_{1-x}Al_xN$ is metastable over a broad concentration range ($0.2 \leq x \leq 0.99$) and undergoes spinodal decomposition. However, one should be careful about interpreting the decomposition of TiAlN seen in Figs. 3 and 4 as a spinodal decomposition process, as a build-up of concentration fluctuations was not observed in-plane. To further elucidate the decomposition process of TiAlN/CrN multilayers, their microstructural evolution upon extended annealing at temperatures between 700 and 1000 °C is currently under investigation.

Annealing at 1000 °C for 1 h causes strong changes in the microstructure of the multilayer coating, as can be seen in the TEM bright and dark-field images in Fig. 5. Apparently, dissolution of the multilayers and grain coarsening correlate with each other and begin at the surface of the coating. Hence, surface-related mechanical properties such as hardness and wear resistance are expected to be substantially deteriorated at this state. APT elemental maps of a sample annealed at 1000 °C for 1 h are presented in Figs. 6 (near-surface region) and 7 (deep region, ~700 nm above the substrate). These APT data are in good agreement with TEM results. Close to the surface, no layered structure is visible. Instead, a coarse domain of pure AlN (more than 100 nm in size) and a domain enriched with Ti and Cr exist. In addition, small nano-sized AlN precipitates can be detected within the Ti and Cr-rich matrix. In the region that is about 700 nm above the substrate, the layered structure is preserved (see Fig. 7). Al-rich layers remain clearly visible while Ti and Cr atoms have partially intermixed. Substantial amounts of Fe (up to 7 at%) and V (up to 1 at%) atoms stemming from the steel substrate can be detected as well. The Fe atoms are enriched in a two-dimensional shape, where the layered structure is perturbed. This Fe rich region most likely marks a columnar grain boundary or a near grain boundary region. Thus, at 1000 °C the grain boundary diffusion is considered as the dominant diffusion

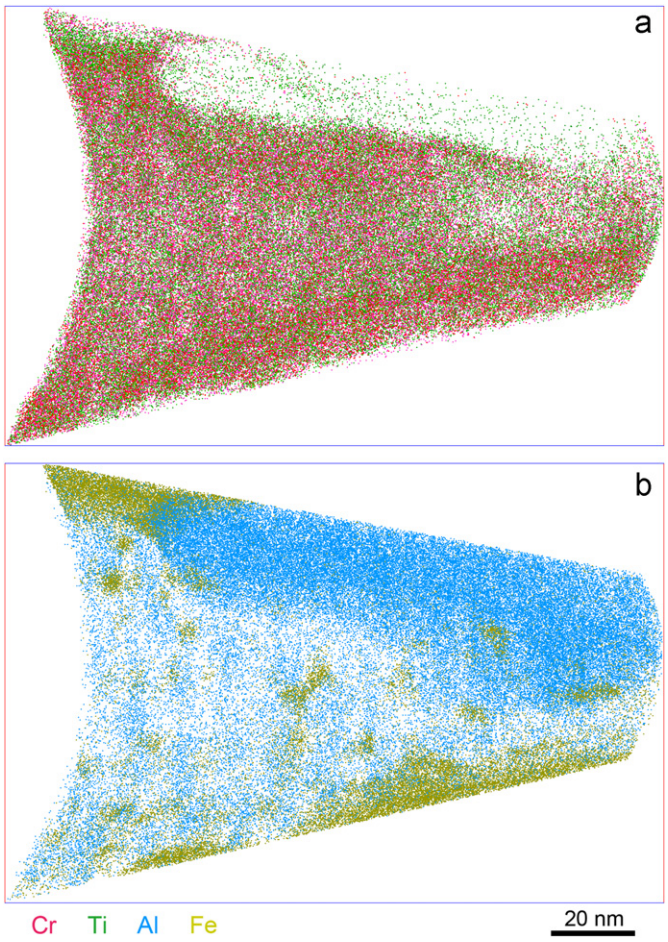

Fig. 6. APT elemental maps for a sample annealed at 1000 °C for 1 h (near-surface region). Nitrogen atoms are not displayed for clarity.

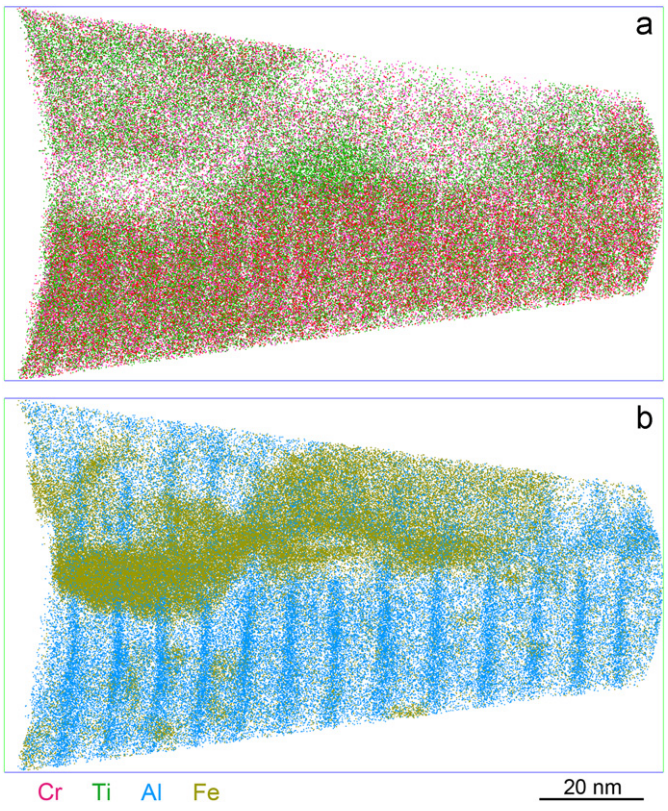

Fig. 7. APT elemental maps for a sample annealed at 1000 °C for 1 h (region about 700 nm above the substrate). Nitrogen atoms are not displayed for clarity.

mechanism for Fe impurities in TiAlN/CrN multilayers. This is because the diffusion coefficient on grain boundaries is typically much larger than that in the bulk. However, when using literature data on grain boundary diffusion of Fe in TiN ($D_0 = 1.4 \times 10^{-15}$ m^2/s, $E_a = 46$ kJ/mol taken from Ref. [35]), the estimated root mean square diffusion distance for 1 h is only about 500 nm. Hence, at first analysis the grain boundary diffusion mechanism alone does not probably explain the presence of considerable amounts of iron in the near-surface region of the coating. Alternatively, it might be possible that additional lattice defects such as an increased impurity-stabilized vacancy concentration or the effect of internal stresses enhance the diffusion rate of iron atoms. Finally, it must be considered that the diffusion coefficients of grain boundaries usually depend on their specific structure and misorientation. This means that, depending on the exact nature of the grain boundary, the actual diffusion coefficient might be higher than the representative value taken from the literature.

4. Conclusions

TiAlN/CrN multilayers of about 9 nm average bilayer period and a Ti:Al ratio of 0.75:0.25 were studied with respect to their thermal stability. The nanolayer structure shows thermal stability up to a temperature of 600 °C. No significant change in the compositional modulation compared to the as-sputtered state is observed at that temperature, though XRD results suggest slight interface broadening due to short-range diffusion. The decomposition of the multilayer structure starts at 700 °C when each TiAlN layer decomposes into a Ti-rich and two Al-rich layers. However, no structural changes occur at that temperature. A further increase in annealing temperature to 1000 °C results in strong changes in the microstructure. Layer dissolution and grain coarsening are correlated with each other and appear to begin at the surface. Significant amounts of Fe and V impurities enter the multilayer coating after heat treatment at 1000 °C via grain boundary diffusion.

Acknowledgement

This work was funded by the German Research Foundation (DFG) (Contract CH 943/1-1).

References

[1] H.J. Holleck, J. Vac. Sci. Technol. A 4 (1986) 2661.
[2] M. Zlatanovic, D. Kakas, L. Mazibrada, A. Kunosic, W.D. Münz, Surf. Coat. Technol. 64 (1994) 173.
[3] M.H. Staia, E.S. Puchi, D.B. Lewis, J. Cawley, D. Morel, Surf. Coat. Technol. 86–87 (1996) 432.
[4] P.C. Yashar, W.D. Sproul, Vacuum 55 (1999) 179.
[5] D.G. Kim, T.Y. Seong, Y.J. Baik, Surf. Coat. Technol. 153 (2002) 79.
[6] M. Shinn, L. Hultman, S.A. Barnett, J. Mater. Res. 7 (1992) 901.
[7] U. Helmersson, S. Todorova, S.A. Barnett, J.E. Sundgren, L.S. Markert, J.E. Greene, J. Appl. Phys. 62 (1987) 481.
[8] Q. Yang, C. He, L.R. Zhao, J.P. Immarigeon, Scripta Mater. 46 (2002) 293.
[9] Q. Yang, L.R. Zhao, J. Vac. Sci. Technol. A 21 (2003) 558.
[10] J.K. Park, Y.J. Baik, Surf. Coat. Technol. 200 (2005) 1519.
[11] J. Lin, J.J. Moore, B. Mishra, M. Pinkas, X. Zhang, W.D. Sproul, Thin Solid Films 517 (2009) 5798.
[12] G.S. Kim, S.Y. Lee, J.H. Hahn, S.Y. Lee, Surf. Coat. Technol. 171 (2003) 91.
[13] U. Bardi, S.P. Chenakin, F. Ghezzi, C. Giolli, A. Goruppa, A. Lavacchi, E. Miorin, C. Paruga, A. Tolstogouzov, Appl. Surf. Sci. 252 (2005) 1339.
[14] S.K. Tien, J.G. Duh, Thin Solid Films 494 (2006) 173.
[15] S.K. Tien, J.G. Duh, J.W. Lee, Surf. Coat. Technol. 201 (2007) 5138.

[16] B.S. Kim, G.S. Kim, S.Y. Lee, B.Y. Lee, Surf. Coat. Technol. 202 (2008) 5526.
[17] I. Wadsworth, I.J. Smith, L.A. Donohue, W.-D. Münz, Surf. Coat. Technol. 94–95 (1997) 315.
[18] D.B. Lewis, I. Wadsworth, W.D. Münz, R. Kunzel Jr., V. Valvoda, Surf. Coat. Technol. 116 (1999) 284.
[19] H. Barshilia, M. Surya Prakash, Anjana Jain, K.S. Rajam, Vacuum 77 (2005) 169.
[20] M. Panjan, S. Sturm, P. Panjan, M. Cekada, Surf. Coat. Technol. 202 (2007) 815.
[21] Q. Luo, W.M. Rainforth, W.-D. Münz, Scripta Mater. 45 (2001) 399.
[22] J.K. Park, H.J. Park, J.H. Ahn, Y.J. Baik, Surf. Coat. Technol. 203 (2009) 3099.
[23] A. Kimura, H. Hasegawa, K. Yamada, T. Suzuki, Surf. Coat. Technol. 120–121 (1999) 438.
[24] M.K. Miller, K.F. Russell, G.B. Thompson, Ultramicroscopy 102 (2005) 287.
[25] K. Thompson, D. Lawrence, D.J. Larson, J.D. Olson, T.F. Kelly, B. Gorman, Ultramicroscopy 107 (2007) 131.
[26] A. Mazor, D.J. Srolovitz, P.S. Hagan, B.G. Bukiet, Phys. Rev. Lett. 60 (1988) 424.
[27] J. Chakraborty, S. Mukherjee, P.M. Raole, P.I. John, Mater. Sci. Eng. A 304–306 (2001) 910.
[28] A. Conde, A.B. Cristóal, G. Fuentes, T. Tate, J. de Damborenea, Surf. Coat. Technol. 201 (2006) 3588.
[29] L.C. Agudelo, R. Ospina, H.A. Castillo, A. Devia, Phys. Scripta T131 (2008) 014006.
[30] L. Hultman, Vacuum 57 (2000) 1.
[31] P.H. Mayrhofer, A. Hörling, L. Karlsson, J. Sjölén, T. Larsson, C. Mitterer, L. Hultman, Appl. Phys. Lett. 83 (2003) 2049.
[32] R. Rachbauer, E. Stergar, S. Massl, M. Moser, P.H. Mayrhofer, Scripta Mater. 61 (2009) 725.
[33] B. Alling, A.V. Ruban, A. Karimi, O.E. Peil, S.I. Simak, L. Hultman, I.A. Abrikosov, Phys. Rev. B 75 (2007) 045123.
[34] B. Alling, I.A. Abrikosov, A. Karimi, J. Appl. Phys. 102 (2007) 044314.
[35] G.I. Grigorov, K.G. Grigorov, M. Stojanova, J.L. Vignes, J.P. Langeron, P. Denjean, L. Ranno, Physica C 241 (1995) 397.